Development of real-time density feedback control on MAST-U in L-mode

Fusion Engineering and Design 202 (2024) 114387

Contents lists available at ScienceDirect

Fusion Engineering and Design

journal homepage: www.elsevier.com/locate/fusengdes

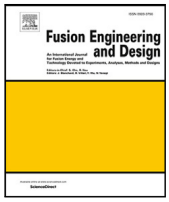

Development of real-time density feedback control on MAST-U in L-mode

G.L. Derks [a,b,*], B. Kool [a,b], C. Vincent [c], S. Elmore [c], S.S. Henderson [c], J.T.W. Koenders [a,b], J. Lovell [e], G. McArdle [c], B. Parry [c], R. Scannell [c], R. Sarwar [c], K. Verhaegh [c,d], M. van Berkel [a], THE EUROFUSION TOKAMAK EXPLOITATION TEAM[1], The MAST-U team[2]

[a] Dutch Institute for Fundamental Energy Research, Eindhoven, Netherlands
[b] Eindhoven University of Technology, Department of Mechanical Engineering, Eindhoven, Netherlands
[c] United Kingdom Atomic Energy Authority, Culham Centre for Fusion Energy, Culham Science Centre, Abingdon, Oxon, United Kingdom
[d] York Plasma Institute, University of York, York, United Kingdom
[e] Oak Ridge National Laboratory, Oak Ridge, USA

ARTICLE INFO

Keywords:
MAST-U
Density
Dynamics
Control

ABSTRACT

In this paper we report on the development and demonstration of density feedback control for MAST-U. Sinusoidal perturbations are used to measure the frequency response from a deuterium gas valve (actuator) to line-integrated core electron density measured by the interferometer (sensor). In the frequency range relevant for control design, only two system-identification experiments were needed to regress a first-order dynamic model. This control-oriented model informs the offline design of a proportional integral controller with the established loop-shaping controller design method. After offline verification of the controller implementation, control is demonstrated by experimentally tracking a staircase reference for the line-integrated electron density. This paper demonstrates the efficiency of controller design using system-identification and loop-shaping, providing reliable density control for MAST-U.

1. Introduction

Magnetic confinement fusion reactors require plasma density control to maximize energy yields and remain within safe operational limits [1–3]. Future reactors will use pellets that penetrate the plasma edge to efficiently fuel the core plasma. On the other hand – in low-confinement (L-mode) experiments – contemporary devices often control the plasma density using gas valves. Neutral Beam Injectors (NBI) are typically employed for heating but also fuel the plasma, affecting density control. Examples reporting on density control with both pellets and gas valves can be found among others for EAST [4], JET [5], ASDEX [6], W7-X [7], DIII-D [8], and TCV [9]. In these devices, density feedback control is essential during daily operations for effective experimentation. The Upgraded Mega Ampére Spherical Tokamak (MAST-U) started operations in the year 2020 and has since operated with a density controller that did not fulfill the needs.

In this paper we develop real-time plasma density feedback control for MAST-U in low confinement (L-mode) plasmas. For the setup in Fig. 1, linearized dynamics are identified between the deuterium gas valve (actuator) and interferometer (sensor) using sinusoidal perturbations at frequencies relevant for control [10]. Based on identified dynamics, we estimate parameters of a control-oriented model which is used to design a proportional integral controller with the loop-shaping method [11]. The controller implementation is verified offline and deployed to experimentally track a staircase reference for the line-integrated core electron density.

The paper is organized as follows. In Section 2, we outline the control problem at hand and investigate characteristics of the hardware. Then, we describe the exact implementation of the controller in the Plasma Control System (PCS). In Section 3, we explain the system identification experiments and extract a control-oriented model. Based on the model, we design and experimentally demonstrate a plasma density controller in Section 4. Section 5 concludes the paper.

2. Control problem characterization

The goal is to control the core plasma density of MAST-U depicted in Fig. 1. It is insufficient to use feedforward control and only prescribe

* Corresponding author at: Dutch Institute for Fundamental Energy Research, Eindhoven, Netherlands.
E-mail address: g.l.derks@differ.nl (G.L. Derks).

[1] See the author list of "Progress on an exhaust solution for a reactor using EUROfusion multi-machines capabilities" by E. Joffrin et al. to be published in Nuclear Fusion Special Issue: Overview and Summary Papers from the 29th Fus. En. Conf. (London, UK, 16–21 October 2023).

[2] See the author list of "Overview of the Physics Results from MAST Upgrade towards core-pedestal exhaust integration" by J.R. Harrison et al. to be published in Nuclear Fusion Special Issue: Overview and Summary Papers from the 29th Fus. En. Conf. (London, UK, 16–21 October 2023).

https://doi.org/10.1016/j.fusengdes.2024.114387
Received 5 December 2023; Received in revised form 28 February 2024; Accepted 20 March 2024
Available online 3 April 2024

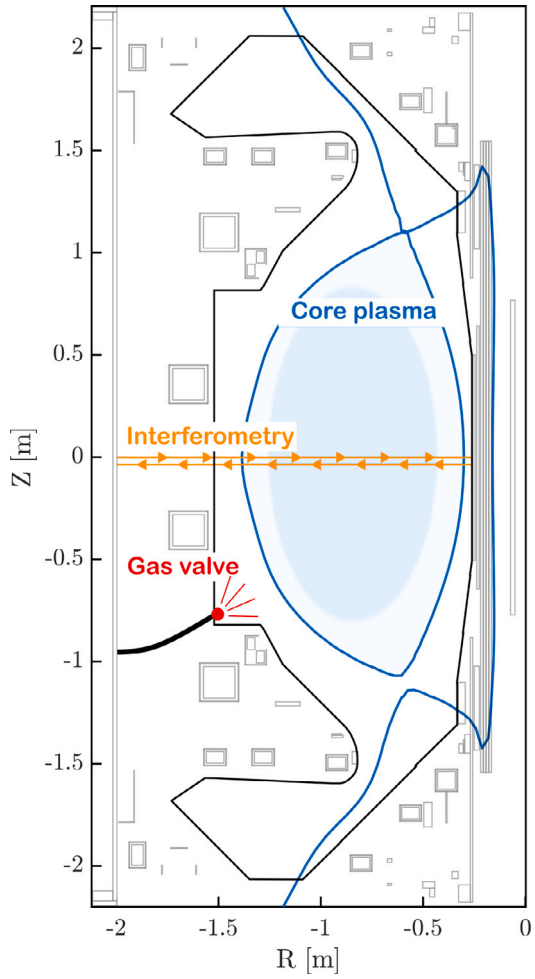

Fig. 1. The experimental setup for core plasma density feedback control at MAST-U. A gas valve at the low field side midplane fuels the core plasma where an interferometer passes through the plasma measuring the line-integrated electron density.

voltages for the gas valve as unknown disturbances cause (random) deviations from the expected outcome, resulting in poor experimental repeatability. To correct for unknown disturbances the valve must be controlled in feedback using information about the electron density from the interferometer. The density control feedback loop is outlined as a block diagram in Fig. 2. The blocks form a local Linear Time Invariant (LTI) approximation of the real system and should be known to design the controller gains. The following subsections investigate components in the control loop that are known a priori.

2.1. Sensor

The sensor $S(s)$ is a single chord, two-color CO2/HeNe laser interferometry system [12]. This diagnostic is used to infer the line-integrated electron density in the core plasma is digitized with a sampling rate of 100 MHz and effective bandwidth of 6 MHz (after real-time processing) [13]. The real-time analogue output used in this work is digitized at 10 kHz. Moreover, it has proven to be reliable over the second campaign of MAST-U (MU02) with an availability of 97.7%, saving data 722 out of 738 discharges. For details on this diagnostic we refer to the original publication in [12].

2.2. Actuator

The actuator is a Piezo-Electric Valve (PEV) located on the low field side midplane of the reactor vessel. The flow request u_F of the controller is transformed into a voltage for the valve u_V by the *flowmixer* M in the plasma control system. The *flowmixer* inverts the following static linear valve calibration:

$$u_F = a u_V + b, \tag{1}$$

where the offset b and slope a are fitted on experiments. In these experiments the vessel is pumped to vacuum, there is no plasma and all pumps are turned off. After this procedure, 200 ms block waves are applied to the piezo electric valve. The block waves have potentials ranging from 30 to 150 V, modifying the opening percentage of the valve and thus gas flow rate.

The flow rates u_F [#/s] are estimated based on pressure measurements p [Pa] of the TG1 pressure gauge as:

$$u_F = \frac{dn}{dt} \cdot V = \frac{V}{kT}\frac{\Delta p}{\Delta t} = \frac{V}{kT}\frac{p_2 - p_0}{t_1 - t_0}. \tag{2}$$

The difference in particle density n [m^{-3}] is multiplied with (empty) vessel volume $V = 50.0$ m^3. Using the ideal gas law, one converts the pressure into a density as $p = nkT$ [Pa], with vessel temperature $T = 394$ K, and Boltzmann constant $k = 1.38 \cdot 10^{-23}$ J K^{-1}. For time t [s], subscripts 0 and 1 denote the beginning and ending of the block voltage applied to the valve. For the pressure, 2 denotes a measurement after t_1 of the TG1 gauge at which the pressure reached an equilibrium. Following the sampling time of 1 Hz for the TG1 gauge, it is not possible to perform dynamic calibrations.

The resulting flow rates as function of potential block wave amplitude are depicted in Fig. 3 for a plenum pressure of approximately 750 and 1510 mbar. A plenum pressure of 750 mbar is used for the system identification and control experiments reported in this work.

As limitation, it should be emphasized that these linear calibrations suffer from inherent inaccuracies: (1) they do not account for hysteresis in the piezo electric valve; (2) they do not consider the non-linear relation between flow rate and valve opening percentage, especially near the closing voltage [14]; (3) no dynamics of valve and gas flow are taken into account. As a result, the 750 mbar calibration predicts zero gas flow at the estimated valve opening potential of 46 V, while in experiments flow can be observed down to potentials of 10 V. However these issues can be resolved as Tokamaks have been equipped with valve assemblies that include pressure transducers and internal control circuits for decades [15]. Such solutions should be considered on MAST-U, possibly including advancements in piezo control [14].

2.3. Controller

The digital control system used for density control at MAST-U operates on sampled signals. This means that continuous Proportional, Integral and Differentiation (PID) control signals – generally used in control design – must be approximated at discrete instances in time [11]. Here we start from the digital controller in the Plasma Control System (PCS) of MAST-U and infer the approximate continuous controller representation that is used for controller design in this paper.

The density control algorithm as implemented in the PCS represents a proportional integral controller with the following discrete difference equation:

$$u_F[k] = K_p e[k] + \frac{K_p}{K_i}\frac{T_s}{10^{-3}} e[k] + u_F[k-1] - K_p e[k-1]. \tag{3}$$

Here the control action u_F [10^{21} #/s] is a particle flow and the error e [10^{21} m^{-2}] is in units of the line-integrated density. The controller is characterized by integrator gain K_i [ms], proportional gain K_p [m^2#/s], and the sample time T_s [s] of the PCS. The error e and control action u_F are evaluated in the present and previous instances k and $k-1$ respectively. Eq. (3) can be transformed into the Z-domain as follows [16]:

$$u_F[z] = K_p e[z] + \frac{K_p}{K_i}\frac{T_s}{10^{-3}} e[z] + e[z]z^{-1} - K_p e[z]z^{-1}, \tag{4}$$

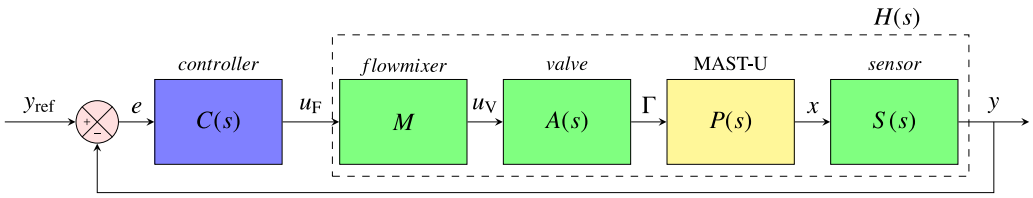

Fig. 2. Schematic of the control loop with the controller $C(s)$ in feedback with system $H(s)$, in the Laplace domain with Laplace variable s. The controller receives error signal e and sends a flow request u_F to the flowmixer which converts this into a voltage u_V for the valve $A(s)$. The valve injects a particle flow Γ into MAST-U $P(s)$ influencing the core plasma density. The plasma density is measured by the interferometry sensor $S(s)$. The output signal of the sensor y is the line-integrated density $\bar{n}_e$ in the plasma. This is subtracted from the reference y_{ref} density to form the error e on which the controller acts.

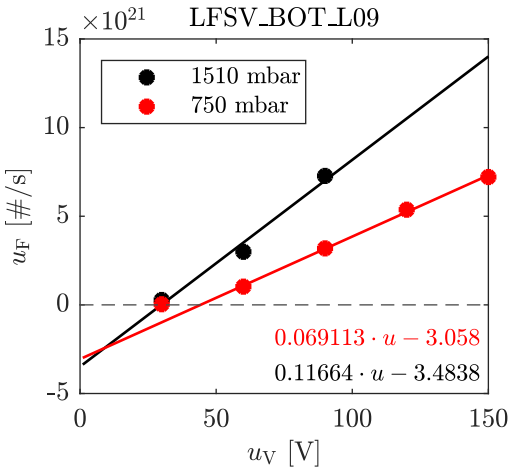

Fig. 3. Calibration of the Low Field Side Vessel Bottom Lower gas valve in sector 09 (LFSV_BOT_L09). Calibrations are performed with plenum pressures of 750 and 1520 mbar. The gas flow rate in particles per second is plotted as function of stationary gas valve potential. Note: this is the calibration as programmed in the Plasma Control System (PCS) and used in experiments discussed in this paper, it is has since been superseded.

where the discrete instances k are replaced by z. Previous instance $k-1$ result in a division by z, representing a discrete shift in discrete time. The controller in Z-domain of Eq. (4) can be rewritten into a transfer function $C[z]$ from error $e[z]$ to flow request $u_F[z]$:

$$C[z] = \frac{u_F[z]}{e[z]} = K_p + \frac{K_p}{K_i 10^{-3}} \frac{T_s z}{z-1}. \tag{5}$$

This is a backward Euler discrete approximation of the following continuous Laplace domain proportional integral controller $C(s)$ [17,18]:

$$C(s) = \frac{U(s)}{E(s)} = K_p + \frac{K_p}{K_i 10^{-3}} \frac{1}{s}, \tag{6}$$

where the discrete backward Euler integrator $\frac{T_s z}{z-1}$ in Eq. (5) is replaced by the ideal integrator $\frac{1}{s}$ in the Laplace domain. This approximation can be used with confidence for controller design in Section 4 as the sample rate of PCS is 10 kHz and more than 25 times the 10 Hz frequencies on which the controller will act. At such respectively high PCS sample rates the approximation error is negligible [11]. Still, the exercise of deriving the transfer function in Eq. (6) from the difference equation in Eq. (3) yields value as it can be seen that a non-negligible unit conversion factor of 10^{-3} is present in the source code of the PCS in MAST-U.

The controller output (flow request) and integrator are clamped to minimum and maximum values to prevent excessive error integration when exceeding actuator limits. The initialization of the integrator is used as a constant feedforward and is set to the flow request known for the controlled valve when control is enabled. The PCS implementation was verified offline and the verification is presented in Appendix A.

Density control on MAST-U is a means to an end. Following delicate scenario requirements, the controller structure allows one to safely use more conservative controller gains (lower K_p or higher K_i). This is already used as session leaders have lowered K_p to lower the proportional response of the controller to internal re-connection events and increased K_i to more gradually approach references and decrease overshoot. The inverse manipulation of the controller gains is not advised as one may destabilize the feedback loop.

3. System identification

In this section we experimentally identify and model the dynamics of $H(s)$ between the flow request u_F and the signal y measured by the interferometer (see also Fig. 2). The experiments feature an L-mode plasma with line-integrated core densities around $\bar{n}_e \approx 1.1 - 2.3 \cdot 10^{20}$ m^{-2}, plasma current of 750 kA and off-axis south-west neutral beam injection with a power in the range of 1.5 MW.

3.1. Perturbative experiments

We use system identification techniques in the frequency domain as specified in [19,20]. We modulate the valve voltage u_V using single sinusoids with frequencies of 7.8 Hz and 20 Hz in respective discharges #46647 and #46648. The frequencies are selected such that the sampling times of the Plasma Control System (PCS), interferometer, and gas valve have one common divider, preventing signal leakage in the frequency domain. Selected frequencies also avoid harmonics at the 50 Hz electrical grid frequency. Moreover, they are fast enough to have at least three perturbation periods during the flat-top of the discharge which is the minimum to determine the standard deviation [19].

The results of system identification discharge #46647 are visible in Fig. 4. The figure shows the correlation of input and output in the time domain and the frequency domain equivalent from the Discrete Fourier Transform (DFT) and Local Polynomial Method (LPM). The magnitude of the output in the frequency domain shows that the signal at the perturbed (excited) frequency is an order of magnitude higher than the noise floor (i.e. signal in non-excited frequencies). On the first frequency bin, around 2 Hz there is a significant signal component above the noise floor that likely originates from detrending the signal with a straight line whereas the transient in the signal is not a perfectly straight line. At unperturbed harmonics of the excited frequency (e.g. at $f = 2f_1$) there is no response above the noise floor which indicates an insignificant non-linear response [20].

The full set of dynamic frequency response measurements are depicted in a Bode diagram in Fig. 5. The errorbars are calculated using the Signal-to-Noise Ratio (SNR). The SNR is defined as $|A|/\sigma_{noise}$ is quantified using the Local Polynomial Method (LPM) [19], which corrects for non-linear transients. The measurements shown in this paper feature a SNR > 5, such that they can be represented by Gaussian distributions in the complex plane [21]. The standard deviation of these Gaussian distributions are used to calculate the 95% confidence intervals that are plotted as errorbars.

The measurements in Fig. 5 represent the system dynamics from the controller perspective, see $H(s)$ in Fig. 2. The controller uses as input

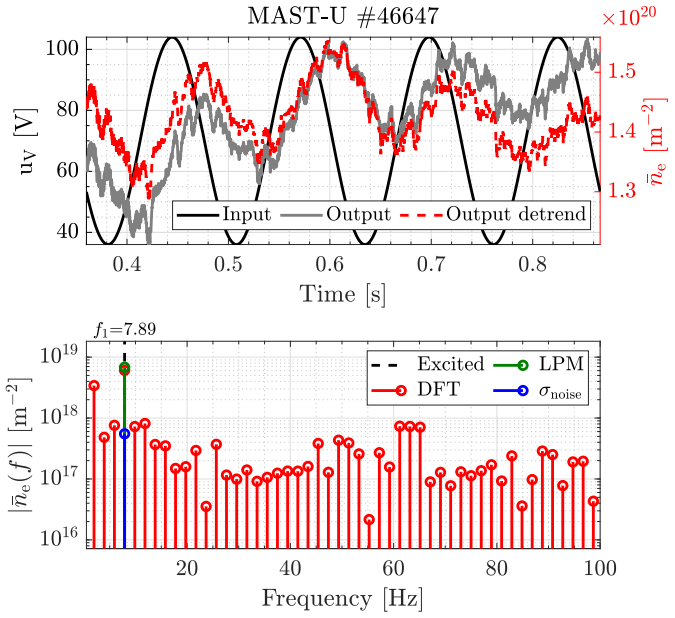

Fig. 4. Frequency response of the line-integrated core density to a modulation of the gas valve potential at 7.89 Hz. In the top, the time domain shows that the period of the sinusoidal input correlates to the output. The bottom depicts the output in the frequency domain obtained with the Discrete Fourier Transform (DFT) taken from the detrended output. For the modulated frequency, the DFT is compared to the Local Polynomial Method (LPM) and its estimate of the noise σ_{noise}.

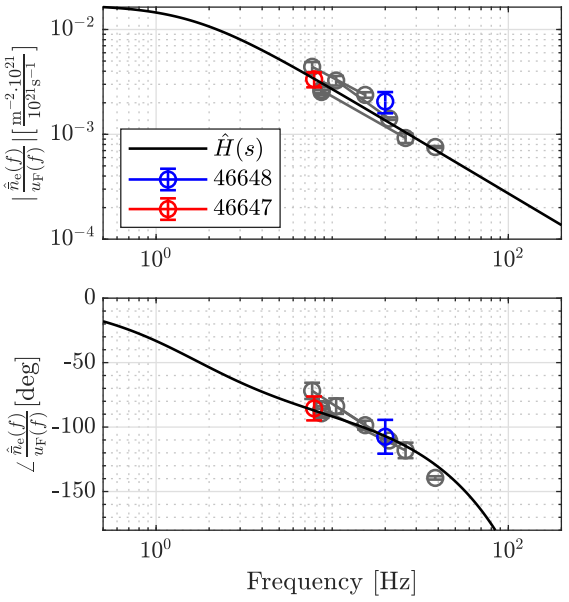

Fig. 5. Model $H(s)$ fitted on frequency responses using Eq. (7). Magnitude (top) and phase (bottom) of the model and FRFs of perturbative experiments obtained with the LPM [19]. The gray data is of discharges #47080, #47083, #47086, #47116, #47118, #47119, performed after density control was established. Similarly, purple and pink results are from respective discharges #49292 and #49294, operating around the highest possible density in this L-mode scenario.

the flow request u_F instead of the valve potential u_V that was modulated in the system identification experiments (due to experimental limitations). To reconstruct the system as seen by the controller, the frequency response measurements are translated from valve potential u_V into requested flow u_F using knowledge of *flowmixer* M. The *flowmixer* M is defined by the static calibration in Eq. (1) of which the factor a is used to map the frequency response measurements from valve potential u_V to flow request u_F. The scaled dynamics are depicted the Bode diagram in Fig. 5, describing the linear attenuation of magnitude and phase in the frequency domain.

3.2. Modeling

To characterize the perturbative experiments, the system dynamics $H(s)$ between flow request u_F and measurement y are modeled as a First-Order Plus Dead Time (FOPDT) transfer function:

$$\hat{H}(s) = \frac{K}{\tau s + 1} \exp(-\tau_d s). \tag{7}$$

Here K [$m^{-2}\#^{-1}$ s] is the gain of the system, τ [s] the characteristic time scale of a response and τ_d [s] a delay. In the case that the static calibrations in M would have been accurate, the model $\hat{H}(s)$ could be valid for other valves with similar dynamics, but with different calibrations.

The experiments do not fully constrain the parameters of the model, especially the steady state gain [22]. Hence, the model is manually aligned with the perturbative system identification experiments resulting in coefficients $K = 1.714 \cdot 10^{-2}$ $m^{-2}\#^{-1}$ s, $\tau = 0.1$ s, and $\tau_d = 3 \cdot 10^{-3}$ s. The steady state gain was deliberately estimated conservatively , meaning smaller than what might be a best guess. Therefore, the low-frequent component of the flow request is expected to be smaller in experiments compared to simulations. Hence, density reference traces can be designed offline that are likely to respect actuator limits in actual experiments. The bode diagram of the fit is visible in Fig. 5. Low frequent (<1 Hz) information can be inferred *from* the control demonstration experiment, tracking a staircase reference in Section 4. Using this information, a best guess for model parameters is presented Appendix D.

3.3. Discussion

A limitation of this model representation is that it is based on a snapshot of the dynamics for a specific scenario and operational day in MAST-U. Therefore, there are no guarantees for this model to represent realistic behavior in other experiments. However, we observe similar dynamics later in the campaign in Fig. 5. In gray, purple, and pink, we appended results of perturbative experiments performed *after* developing density control. These post-modeling measurements are consistently close to the model and show that the L-mode scenario for which $H(s)$ was identified behaved similarly across discharges of two separate campaigns, for densities near $\bar{n}_e \approx 1.1 \cdot 10^{20}$ m^{-2} (gray) and $\bar{n}_e \approx 2.3 \cdot 10^{20}$ m^{-2} (for purple and pink). Additionally, Fig. 4 shows an insignificant non-linear response at unperturbed frequencies. These observations suggest that the dynamics of the core density response to the gas valve in this L-mode scenario are predominantly linear [23], that is, in the 7–40 Hz frequency range of the measurements. Further details on time traces and magnetic equilibria of the experiments are presented in Appendix B.

4. Control design and demonstration

In this section the two system identification experiments are used to design a controller which is demonstrated to track a staircase reference for the line-integrated core plasma density. Here we do not consider interactions with other closed loops, but this is likely required when developing simultaneous control of e.g. the plasma exhaust and core [9].

4.1. Design

Using the model derived from experiments $\hat{H}(s)$, we systematically design a controller with the loop-shaping method [11]. We shape

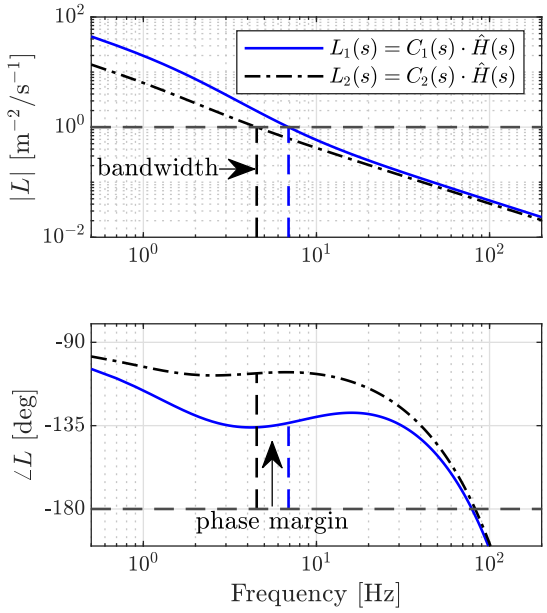

Fig. 6. The open loops L_1 and L_2 used in respective controller designs: $C_1(K_i = 20$ ms, $K_p = 170$ m^2#/ s) and $C_2(K_i = 58$ ms, $K_p = 150$ m^2#/ s). The second controller features a lower bandwidth (less performance) but more phase margin (more stability guarantees). Controller C_1 was used in the simulation and experiment in Fig. 7.

the open loop transfer function $L(s) = C(s)\hat{H}(s)$ to obtain a desired bandwidth and phase margin, respectively representing performance and stability. The bandwidth ω_{bw} [rad/s] is defined as the frequency where the open loop magnitude is unity $|L(s = i\omega_{bw})| = 1$ and the phase margin is the angle in the complex plane between minus one (−1,0) and $L(i\omega_{bw})$.

To illustrate the loop-shaping process, Fig. 6 depicts two controller designs $C_{1,2}$ with their open loop transfer function $L_{1,2}$ and corresponding bandwidth and phase margin. When shaping L, one has to make a trade-off between bandwidth and phase margin. The phase margin should typically lie between −30 and −90 degrees to ensure stability, where higher phase margins reduce overshoot in reference tracking at the cost of performance. On the other hand, higher bandwidths typically result in faster rise times, e.g. time to reach 90% of a step reference. This trade-off is clearly visible between $L_{1,2}$.

As final controller design we select C_1 because it features a bandwidth of 7 Hz that is close to measurement data at 7.8 Hz. This measurement has a 20 degrees errorbar on phase that guarantees closed loop stability with a probability of over 99%. This stability guarantee is driven by the small errorbar of the measurement, providing an accurate system representation at a single frequency.

The expected performance of controller C_1 was simulated for a staircase density reference *before* doing an experimental demonstration. This (closed loop) simulation is depicted as a dashed-dotted line in Fig. 7 and represents the block diagram in Fig. 2 using the model $\hat{H}(s)$. There is overshoot in this simulation and one could choose to use controller C_2 to reduce overshoot as it has more phase margin, albeit at the cost of lower bandwidth. For the interested reader, the expected tracking performance of C_2 is presented in Appendix C.

4.2. Demonstration

Finally, we deploy the controller C_1 on MAST-U in discharge #46813. In this experiment, the plasma is initiated with a pre-set waveform on a high field side midplane valve. The feedforward signal on the controlled low field side valve is set by a sample and hold of the flow request as control is enabled, around 0.15 s. From there the feedback controller is assigned to track a staircase reference for the line-integrated plasma density.

Results from the experimental demonstration of density feedback control are visible in Fig. 7 along with the simulated expectation. The experimental trace follows the expected one closely and approaches the reference. However, in the experiment the first step has more overshoot than expected. This may be caused by the density dropping slightly just before the step, resulting in a larger change of reference than in the simulation. Simultaneously, it is likely due to model mismatches underestimating the gain at low densities. Another model mismatch is the omission of a clamp on the controller, where in the experiment the valve voltage was clamped at 0.4 s and limited to 150 V. The clamp is not used in simulation because the model was not informed by measurements at low frequencies and the predicted required flow to maintain a density (steady state gain) was selected conservatively, likely overestimated. An extended analysis is presented in Appendix D.

4.3. Discussion

A major merit of feedback control is that it attenuates low-frequent model inaccuracies and disturbances. Suppose that the actual system dynamics are given by $H = \hat{H} + \delta\hat{H}$, where $\hat{H}$ is the model and $\delta\hat{H}$ is the modeling error. The implications of this modeling error for tracking performance can be evaluated using the sensitivity function S, i.e. transfer function from reference y_{ref} to tracking error e:

$$S = \frac{e}{y_{\text{ref}}} = \frac{1}{1 + \hat{H}C_1} = \frac{1}{1 + L_1}. \tag{8}$$

The sensitivity function determines the extend in which modeling errors express themselves in the closed loop transfer function $T = y/y_{\text{ref}} = \hat{H}C_1/(1 + \hat{H}C_1) = L_1/(1 + L_1)$ [11]. Suppose the model error $\delta\hat{H}$ is 10% at a frequency of 1 Hz. We find in Fig. 6 that L_1 has a magnitude of 20 at 1 Hz and the sensitivity has a value of $S = 1/21$. Consequently, the model error $\delta\hat{H}$ of 10% in magnitude will only cause a 0.5% change in the magnitude of the closed loop transfer function T (see also Section 4.1.4 in [11]). In this way, feedback significantly reduces the sensitivity of $T = y/y_{\text{ref}}$ to model errors in $\hat{H}$ for regions where the open loop gain L_1 is large, i.e. below the bandwidth.

The above property of feedback is exploited in developing a controller with the purpose of tracking a staircase reference. If one transforms the steps in the staircase reference from the time-domain to the frequency domain, one finds that the power of the signal is distributed with frequency f as $1/f$. This means that the staircase reference predominantly excites low frequencies, i.e. below the bandwidth. In our time-domain simulations, we thus simulate a low-frequency part of the model for which the accuracy is likely poor. Naturally, the required actuation is very different in simulation and experiment as the controller acts on systems with different dynamics and no disturbances, tracking the same reference. If one aims to predict the exact actuation required to obtain a staircase reference (i.e. perfect control in feedforward), one thus requires an accurate model in the low-frequency range. However, using a feedback controller with guarantees on stability and bandwidth, low-frequent model uncertainties are attenuated and good reference tracking can be achieved without an accurate low-frequent model representation.

5. Conclusion & discussion

Systematic model-based density feedback control is demonstrated on MAST-U. Following [10,24–26], this paper illustrates the ease with which systematic methods can be used to promptly establish feedback control - in this case requiring only two discharges and principles of feedback. A key demonstration in this paper is visible in Fig. 7 where the controller is used to track a staircase reference for the line-integrated plasma density covering a large range from $\bar{n}_e \approx 1 - 2 \times$

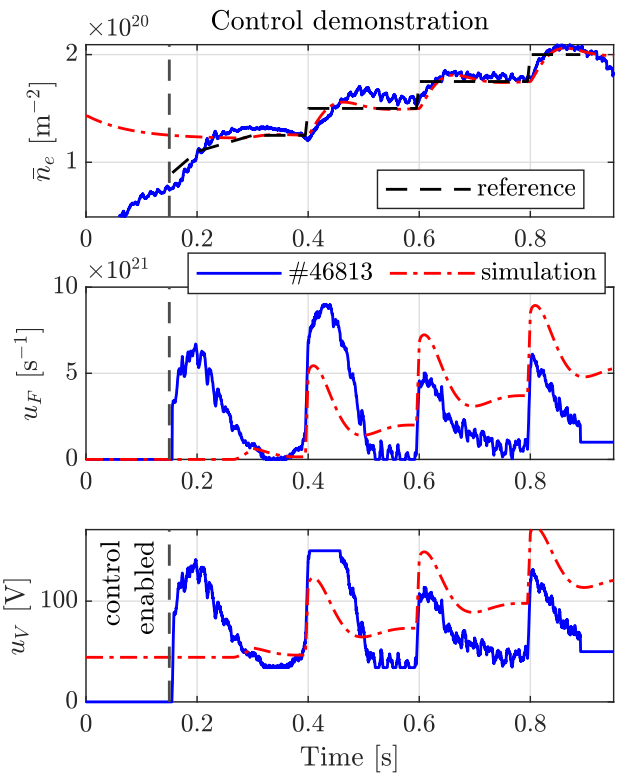

Fig. 7. Closed loop simulation and experiment #46813 tracking a reference density (top) using a flow request (middle) translated into a voltage (bottom) applied to the LFSV_BOT_L09 valve by the flowmixer in PCS. The controller C_1 uses settings $K_i = 20$ and $K_p = 170$. Plasma startup is performed in feedforward by specifying the voltage for a high field side midplane valve in sector 2 (HFS_MID_U02).

10^{20} m^{-2}. In terms of epistemic value, the system-identification experiments show that the dynamics of the line-integrated core density in this L-mode scenario on MAST-U is predominantly linear and invariant to the electron density of the scenario in a frequency range of 7 Hz to 40 Hz.

It is important to note that the results in this paper require a reliable real-time sensor together with an actuator that is fast enough to act on the system dynamics and disturbances. Moreover, the characteristics of the hardware and the exact implementation of the controller in the control system should be known to properly configure the feedback controller. That is also why this work includes details on gas calibration, controller implementation and PCS verification.

A limitation is that, strictly speaking, control performance and stability are only guaranteed in the scenario (L-mode) and around the density for which the system-identification experiments are performed, i.e. $\bar{n}_e \approx 1.5 \times 10^{20}$ m^{-2}. However, the phase margin guards stability and leaves room for small changes in the dynamics of the scenario. As such, the demonstration in 7 covered a range from the minimum (at lower densities strike point splitting triggers a protection probe) to almost maximum density (disruption due to density limit). Moreover, the density controller has been used in Ohmic discharges and with different divertor configurations using the more conservative controller C_2. The controller C_2 has also been used with other valves, however, caution is advised when using valves with significantly longer delays – e.g. due to longer piping – as delays can easily diminish the phase margin [11,18]. For example, the presented 7 Hz bandwidth with 45 degrees ($\pi/2$ radian) only allow an additional delay of $\tau_d = \theta/(2\pi f) = 0.5\pi/(2\pi \cdot 7) = 17.9$ ms before destabilizing the closed feedback loop. Finally, density control is also used in H-mode experiments to save the plasma in case of unforeseen L-H transitions (e.g. experiment #48898). In this case the session leader selects a low density reference and disables the integrator $K_I \to \infty$ to make the response direct and tractable.

The work presented in this paper strongly connects to recent developments on the TCV Tokamak to control the exhaust [24,26]. These developments heavily rely on data-based dynamic exhaust models since physics-based counterparts are in their infancy [22,27,28]. This is notably different for the control of the core density (profile) where physics-based dynamic models are already present in literature and employed on devices and in simulations [29,30]. A rigorous validation in the frequency domain based on system-identification data seems to be missing. Once validated, both data and physics based dynamic models can be used with confidence through established control design techniques [11,18]. In this work a data-based control-oriented model is identified and exploited for control design. The gathered data allows for validation of physics-based models, e.g. as performed for edge transport using a single blockwave frequency in [31], this is left as future work.

Future work on MAST-U should focus on the dynamic identification of the gas flow entering the vessel. As a result in-vessel dynamics can be separated from the pipe and valve dynamics. This will greatly enhance physics interpretability and allow for proper cross-machine comparison and ultimately extrapolation to future devices.

CRediT authorship contribution statement

G.L. Derks: Writing – review & editing, Writing – original draft, Methodology, Investigation, Formal analysis, Conceptualization. **B. Kool:** Writing – review & editing, Visualization, Software, Methodology, Investigation, Formal analysis. **C. Vincent:** Writing – review & editing, Supervision, Resources, Investigation. **S. Elmore:** Validation, Supervision, Resources, Methodology, Investigation, Formal analysis. **S.S. Henderson:** Methodology. **J.T.W. Koenders:** Writing – review & editing, Supervision, Methodology. **J. Lovell:** Supervision. **G. McArdle:** Supervision, Software, Resources. **B. Parry:** Supervision, Software, Resources, Methodology, Data curation. **R. Scannell:** Supervision, Software, Resources, Data curation. **R. Sarwar:** Software, Resources, Data curation. **K. Verhaegh:** Supervision, Resources, Project administration, Investigation, Data curation. **M. van Berkel:** Writing – review & editing, Supervision, Software, Resources, Project administration, Methodology, Funding acquisition, Formal analysis, Data curation, Conceptualization.

Declaration of competing interest

The authors declare that they have no known competing financial interests or personal relationships that could have appeared to influence the work reported in this paper.

Data availability

Data will be made available on request.

Acknowledgments

DIFFER is part of the institutes organization of NWO. This work has been carried out within the framework of the EUROfusion Consortium, partially funded by the European Union via the Euratom Research and Training Programme (Grant Agreement No 101052200 — EUROfusion). Views and opinions expressed are however those of the author(s) only and do not necessarily reflect those of the European Union or the European Commission. Neither the European Union nor the European Commission can be held responsible for them.

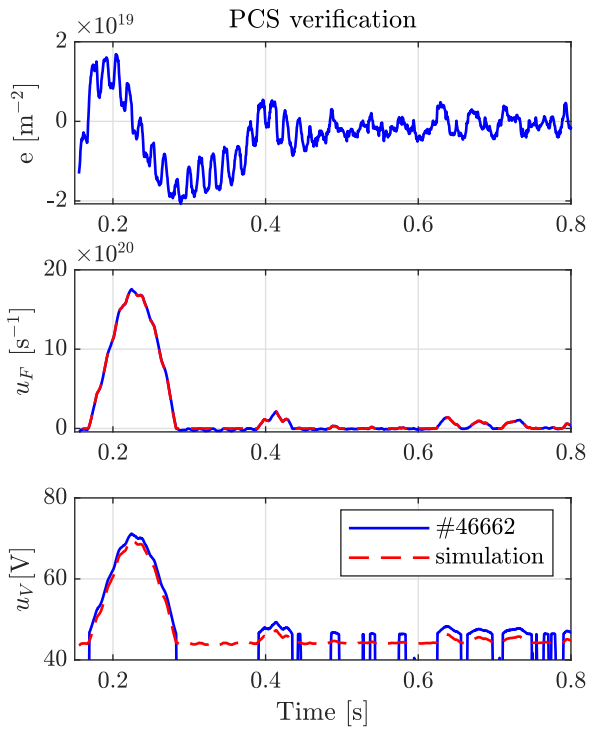

Fig. A.8. Verification of the plasma control system implementation. The error on the density in an experiment with feedback control (top) are used to reproduce traces for requested flow (middle) and valve voltage (bottom). Experimental traces are in blue and simulated traces are in orange.

Appendix A. Controller verification

The control implementation is verified in discharge #46662 in MAST-U. The integral action is set to $K_i = 1$ ms and the proportional action to $K_p = 3$ m^2#/ s. The goal is to verify if the internal PCS signals are similar to the description in this letter. This verification is done in the background during another experiment, does not require the feedback controller to actually control the valve, and does not cost experimental time. Results are depicted in Fig. A.8. It can be seen that the requested flow is perfectly reproduced while the valve voltage is almost perfectly matched. There is one notable discrepancy visible in the lowest voltage, which suddenly drops in the experiment while it is constant in simulation. This is caused by the *flowmixer* (see Fig. 2), which closes the valve when zero flow is requested.

Appendix B. Auxiliaries perturbation experiments

This section presents additional data for the system identification experiments to provide more background on the plasma and machine conditions. In Fig. B.9, the magnetic equilibria from EFIT show that system identification experiments where conducted for divertor plasma configurations ranging for a strike point at small to large radius in a conventional (CD) configuration, moving radially out to the elongated (ED) and eventually super-X (SXD) configuration.

Further detailing the system identification experiments, Figs. B.10 and B.11 depict time traces for: the used valve potential; line integrated plasma density; plasma current; and injected NBI power. The perturbations applied to the gas valve covering the entire actuation range from 0 V to 150 V. The densities around which these perturbations are applied also cover the operating range of MAST-U going from $1 \cdot 10^{20}$ m^{-2} up to $2.5 \cdot 10^{20}$ m^{-2}, which is approximately the limit for this L-mode scenario. There is one experiment where the on-axis NBI was turned on just after 400 ms, resulting in an H-mode around 630 ms with accompanied uncontrolled density ramp ending in a disruption.

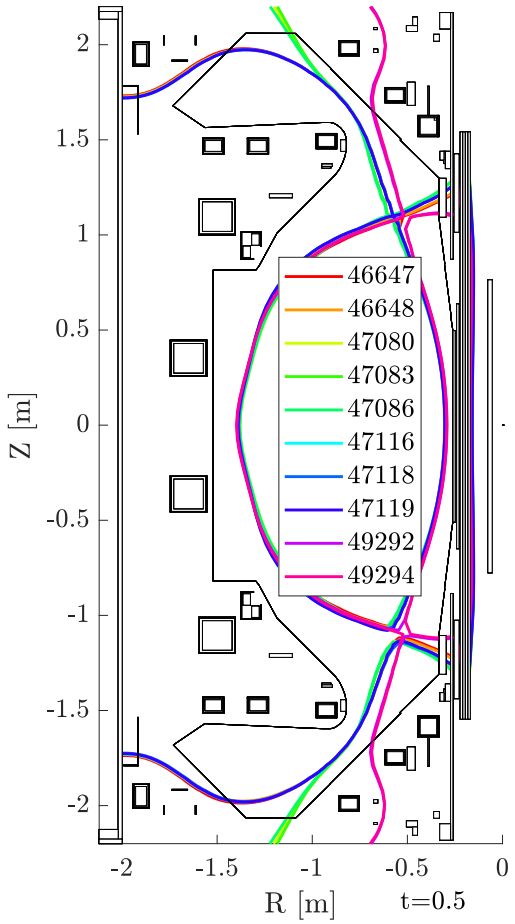

Fig. B.9. Magnetic equilibria of system identification experiments with configurations in CD: 49292, 49294; in ED: 47080 47083, 47086; and in SXD: 46647, 46648, 47118, 47119. Not all colors are clearly visible demonstrating also the repeatability of the magnetic configuration. Time traces are visible in Figs. B.10 and B.11.

Appendix C. Simulated controller comparison

Although in principle the methodology of controller design is in the frequency domain, it is possible to obtain an idea of the control performance in the time domain. This was illustrated in Fig. 7 for controller C_1. In this appendix we also show the expected performance in the time domain for C_2. This is visible in Fig. C.12, based on which session leaders can make an informed decision on which controller should be used.

Appendix D. Extended control experiment analysis

In this section we provide an extended analysis regarding the modeling for experimental results. The starting point of this analysis is the large discrepancy in Fig. 7 between the control action u_F in the experiment and simulation. In this work two possible explanations are proposed: (1) disturbances, for instance around 0.4 s; and (2) modeling errors. Here we substantiate those explanations analytically and through numerical simulations.

First we investigate the traces of Fig. 7 (copied here in Figure) in detail to argue that although the discrepancies are large, they are not unreasonable in the presence of a disturbance. We copied Fig. 7 in Fig. D.13 and also present the tracking errors of experiment and simulations in Fig. D.14. Starting at 0.4 s, where some disturbance causes a dip in density which increases the error from $25 \cdot 10^{18}$ m^{-2} to $30 \cdot 10^{18}$ m^{-2}. In the control response the proportional action in the simulated flow request u_F is 115 V while it is 20% higher in the experiment

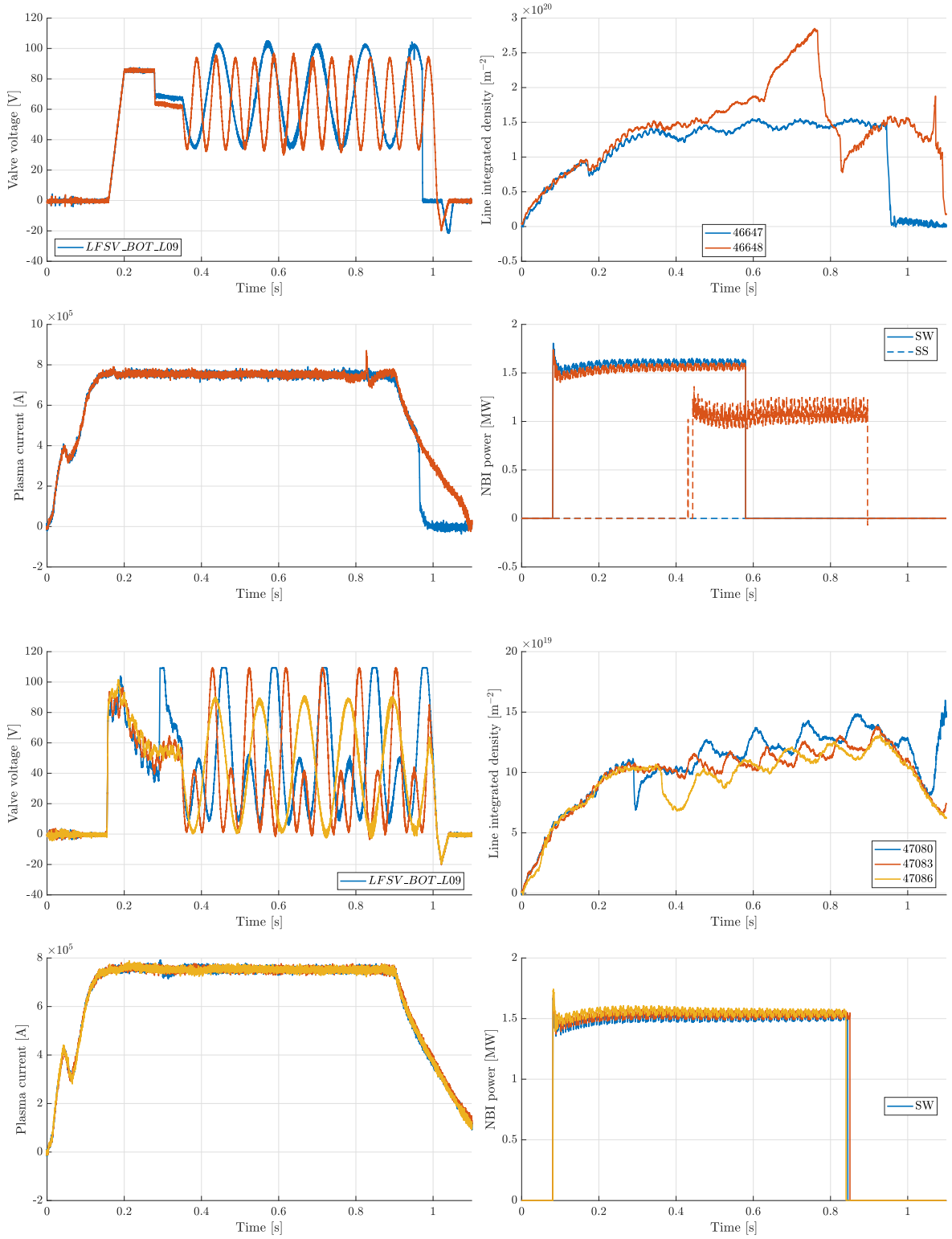

Fig. B.10. The time traces of two sets of system identification experiments (top and bottom blocks of four). On display are: (top left) the potential applied to the LFSV_BOT_L09 valve during the shots; (top right) the line-integrated density evolving between $100 \cdot 10^{18}$ m^{-2} and $300 \cdot 10^{18}$ m^{-2}; (bottom left) the plasma current at 750 kA during the flat top phase; (bottom right) the South-West (SW) off-axis Neutral Beam Injector (NBI) repeatedly injecting 1.5 MW and one shot with South-South (SS) on-axis injection. The magnetic equilibria are depicted in Fig. B.9.

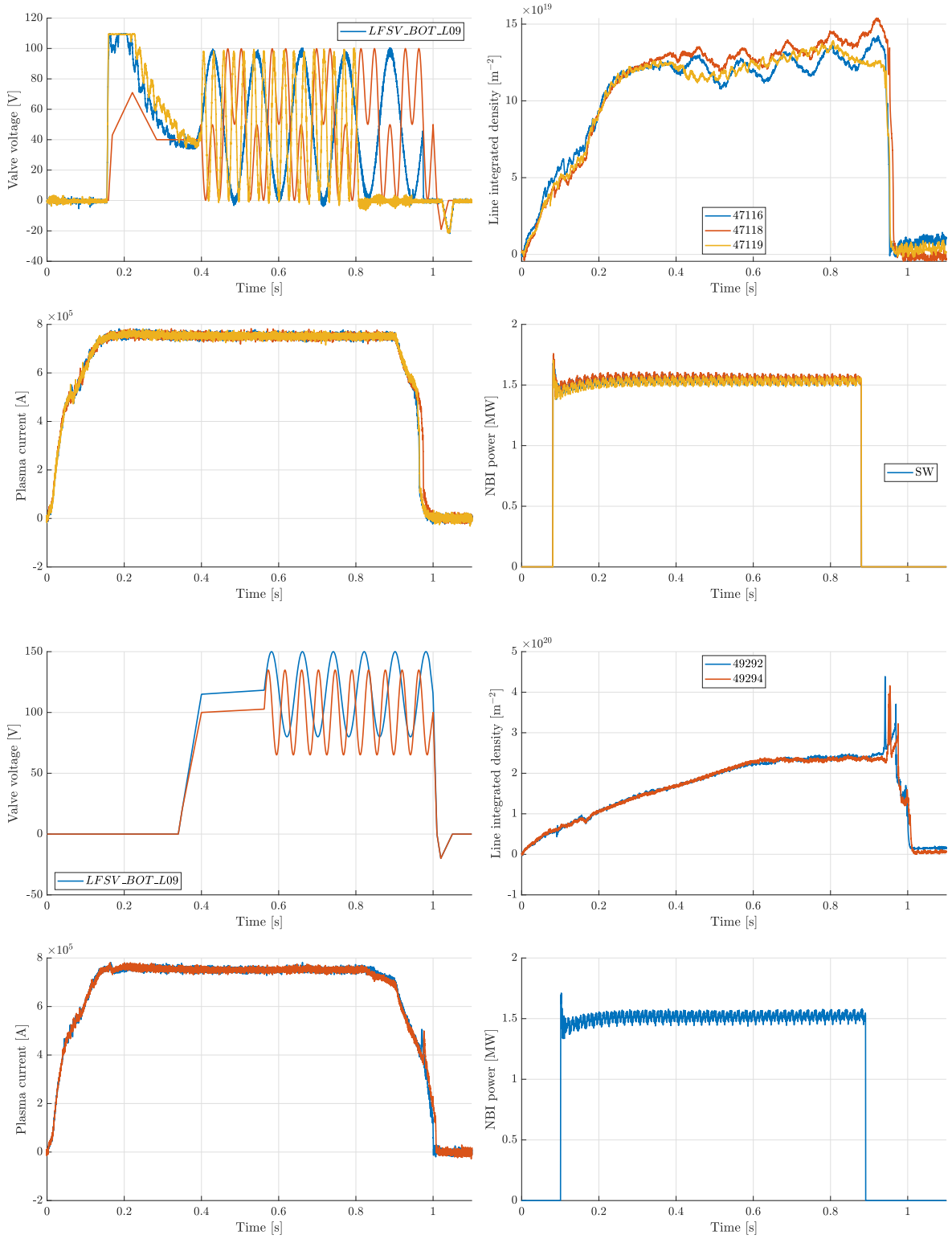

Fig. B.11. The time traces of two sets of system identification experiments (top and bottom blocks of four). On display are: (top left) the potential applied to the LFSV_BOT_L09 valve during the shots; (top right) the line-integrated density evolving between $100 \cdot 10^{18}$ m^{-2} and $300 \cdot 10^{18}$ m^{-2}; (bottom left) the plasma current at 750 kA during the flat top phase; (bottom right) the South-West (SW) off-axis Neutral Beam Injector (NBI) repeatedly injecting 1.5 MW. Unfortunately the NBI data for #49294 was not saved. The magnetic equilibria are depicted in Fig. B.9.

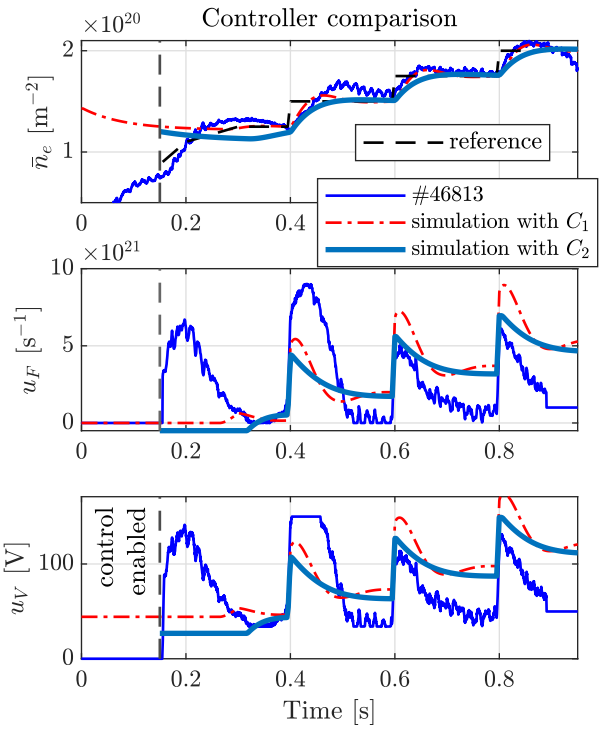

Fig. C.12. A comparison of expected tracking performance in the time domain between controller designs C_1 and C_2 (see also Fig. 6). In addition the experimental result obtained with C_1 are displayed.

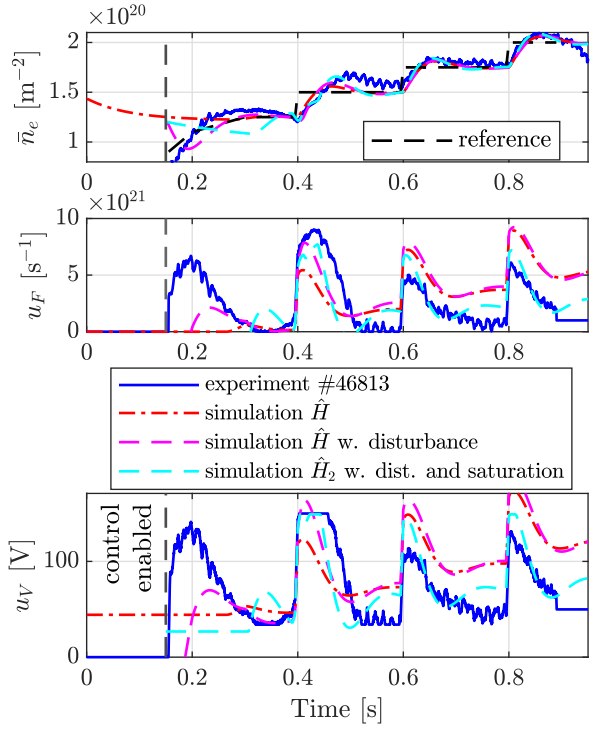

Fig. D.13. A copy of Fig. 7 with the addition of closed loop simulations that include: (1) an output disturbance around 0.4 s; and additionally (2) a more realistic model $\hat{H}_2$ with actuator saturation. Note that the closed loop system includes the controller C_1 and feedback loop as presented in Fig. 2. Changes are made to the model used for H in the simulation and an output disturbance is summed to the output y before calculating the error. The errors are depicted in detail in Fig. D.14.

around 142 V, corresponding to the larger error in the experiment. In the subsequent milliseconds, the integrator consequently collects a larger area from the error in the experiment compared to simulation and takes longer to reach the reference. It is not unreasonable for this discrepancy to explain the roughly 66% difference in peak flow request in the experiment compared to simulation.

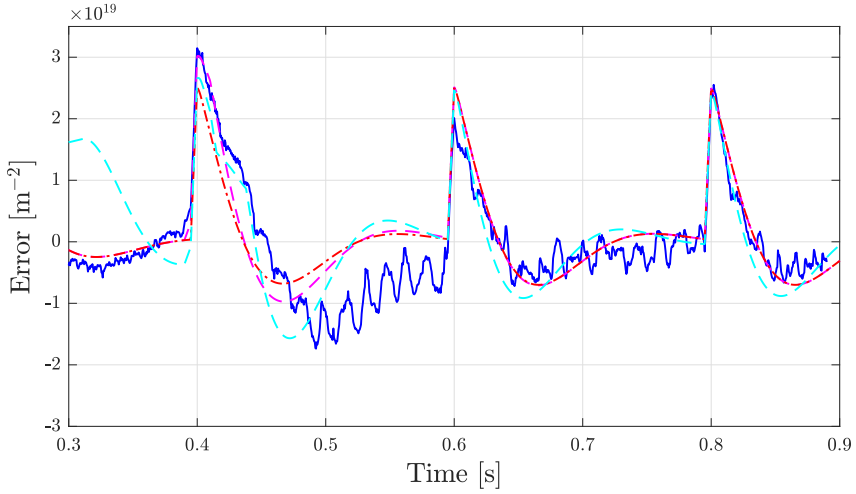

Fig. D.14. The errors as function of time in closed loop simulations and experiments of Fig. D.13.

Secondly we simulate the closed loop behavior of the system. We include a disturbance around 0.4 s and forge the solution to go down by $11 \cdot 10^{18}$ m^{-2}. The introduced disturbance could have a connection with magneto hydrodynamic (MHD) activity in the core plasma. Around 360 ms there is a mode appearing and slowing down from 3 kHz to 1 kHz on the magnetics spectrogram (not shown). Moreover, it appears that around 360 ms the q = 1 flux surface enters the plasma, something that is consistent with a rollover in Soft XRay (SXR) emission (from a diode looking through the center of the core). In Fig. D.13 the outcome of this simulation with a disturbance can be seen in magenta. Clearly the initial response of the controller in the first step is much more aligned with the experiment. In addition, the model is re-aligned based on the outcome of the control demonstration. This re-aligned model is called $\hat{H}_2$ and is based on values $K = 4.3 \cdot 10^{-2}$ m^{-2}#$^{-1}$s, $\tau = 0.2$ s, and $\tau_d = 3.5 \cdot 10^{-3}$ s. We also add an actuator saturation around 150 V as present in the experiment and add a disturbance around 0.42 seconds reducing the density by another $24 \cdot 10^{18}$ m^{-2} in addition to the disturbance introduced earlier around 0.4 s. The outcome of a new closed loop simulation is visible in cyan. It can be seen that the actuator also saturates and starts to align with the experimental response in the first step of the staircase. Moreover, it can be seen that the response in the second and third step dropped significantly, that is because the steady state gain of the new model $\hat{H}_2$ is higher compared to $\hat{H}$.

In terms of a physical interpretation, the value for τ can be seen as a particle confinement time, whereas the input is delayed by τ_d:

$$\frac{d\bar{n}_e(t)}{dt} = -\frac{1}{\tau}\bar{n}_e(t) + c_0 u_F(t - \tau_d). \tag{D.1}$$

Taking the Laplace transform, ignoring initial conditions, and incorporating the constant c_0 into $K = c_0\tau$, one retrieves in the transfer function of Eq. (7). From the model parameters presented in this appendix, the particle confinement time is estimated to be around 200 ms in the L-mode scenario reported on in this paper. The delay is ascribed to the gas flow from valve through the pipe into the vessel and is estimated to be a few milliseconds.

References

[1] T.O. Bosman, O. Kudláček, E. Fable, M. van Berkel, F. Felici, A. Bock, T. Luda, M.R. de Baar, Kalman filter density reconstruction in ICRH discharges on ASDEX upgrade, Fusion Eng. Des. 170 (April) (2021) http://dx.doi.org/10.1016/j.fusengdes.2021.112510.

[2] M. Siccinio, W. Biel, E. Fable, T. Franke, F. Janky, P.T. Lang, M. Mattei, F. Maviglia, F. Palermo, O. Sauter, M.Q. Tran, S. Van Mulders, H. Zohm, Impact of the plasma operation on the technical requirements in EU-DEMO, Fusion Eng. Des. 179 (July 2021) (2022) 113123, http://dx.doi.org/10.1016/j.fusengdes.2022.113123.

[3] H. Zohm, F. Militello, T.W. Morgan, W. Morris, H. Reimerdes, M. Siccinio, The EU strategy for solving the DEMO exhaust problem, Fusion Eng. Des. 166 (January) (2021) 112307, http://dx.doi.org/10.1016/j.fusengdes.2021.112307.

[4] Q. Yuan, B. Xiao, B. Penaflor, D. Piglowski, L. Liu, R. Johnson, M. Walker, D. Humphreys, New achievements in the EAST plasma control system, Fusion Eng. Des. 85 (3–4) (2010) 474–477.

[5] M. Lennholm, T. Budd, R. Felton, M. Gadeberg, A. Goodyear, F. Milani, F. Sartori, Plasma control at JET, Fusion Eng. Des. 48 (1–2) (2000) 37–45.

[6] W. Treutterer, R. Cole, K. Lüddecke, G. Neu, C. Rapson, G. Raupp, D. Zasche, T. Zehetbauer, A.U. Team, ASDEX Upgrade Discharge Control System—A real-time plasma control framework, Fusion Eng. Des. 89 (3) (2014) 146–154.

[7] C. Beidler, Y. Feng, J. Geiger, F. Köchl, H. Maßberg, N. Marushchenko, C. Nührenberg, H. Smith, Y. Turkin, (Expected difficulties with) density-profile control in W7-X high-performance plasmas, Plasma Phys. Control. Fusion 60 (10) (2018) 105008.

[8] P. Gohil, T. Evans, J. Ferron, R. Moyer, C. Petty, K. Burrell, T. Casper, A. Garofalo, A. Hyatt, R. Jayakumar, et al., Control of plasma profiles in DIII-D discharges, Plasma Phys. Control. Fusion 48 (5A) (2006) A45.

[9] J. Koenders, A. Perek, C. Galperti, B. Duval, O. Février, C. Theiler, M. van Berkel, T. Team, et al., Systematic design of a multi-input multi-output controller by model-based decoupling: a demonstration on TCV using multi-species gas injection, Nucl. Fusion 63 (10) (2023) 106007.

[10] M. Van Berkel, A. De Cock, T. Ravensbergen, G.M. Hogeweij, H.J. Zwart, G. Vandersteen, A systematic approach to optimize excitations for perturbative transport experiments, Phys. Plasmas 25 (8) (2018) 1–14, http://dx.doi.org/10.1063/1.5010325.

[11] G.F. Franklin, J.D. Powell, A. Emami-Naeini, Feedback Control of Dynamic Systems, Vol. 33, Pearson London, 2015.

[12] T. O'Gorman, G. Naylor, R. Scannell, G. Cunningham, K. Brunner, R. Martin, D. Croft, Design of a real-time two-color interferometer for MAST Upgrade, Rev. Sci. Instrum. 85 (11) (2014).

[13] K.J. Brunner, T. O'Gorman, G. Naylor, R. Scannell, G. Cunningham, R. Sharples, N.A. Dipper, FPGA-based high bandwidth integral electron density interferometer for MAST-U, PoS ECPD2015 (2016) 138, http://dx.doi.org/10.22323/1.240.0138.

[14] J.B. Liseli, J. Agnus, P. Lutz, M. Rakotondrabe, An overview of piezoelectric self-sensing actuation for nanopositioning applications: Electrical circuits, displacement, and force estimation, IEEE Trans. Instrum. Meas. 69 (1) (2019) 2–14.

[15] S.C. Bates, K.H. Burrell, Fast gas injection system for plasma physics experiments, Rev. Sci. Instrum. 55 (6) (1984) 934–939, http://dx.doi.org/10.1063/1.1137845.

[16] L.B. Jackson, The z transform, in: Digital Filters and Signal Processing, Springer, 1996, pp. 29–54.

[17] R.J. Beerends, H.G. ter Morsche, J. Van den Berg, E. Van de Vrie, Fourier and Laplace transforms, 2003.

[18] S. Skogestad, I. Postlethwaite, Multivariable Feedback Control: Analysis and Design, John Wiley & Sons, 2005.

[19] M. Van Berkel, R. Van Kampen, G. Vandersteen, T. Kobayashi, T. Ravensbergen, H. Igami, J. Lammers, G. Oosterwegel, C. Galperti, F. Felici, et al., Correcting for non-periodic behaviour in perturbative experiments: application to heat pulse propagation and modulated gas-puff experiments, Plasma Phys. Control. Fusion 62 (2020) 094001.

[20] R. Pintelon, J. Schoukens, L. Pauwels, E. Van Gheem, Diffusion systems: Stability, modeling, and identification, Conf. Rec. - IEEE Instrum. Meas. Technol. Conf. 2 (1) (2005) 894–899, http://dx.doi.org/10.1109/imtc.2005.1604264.

[21] M. Van Berkel, H.J. Zwart, G. Hogeweij, G. Vandersteen, H. Van Den Brand, M. De Baar, A.U. Team, et al., Estimation of the thermal diffusion coefficient in fusion plasmas taking frequency measurement uncertainties into account, Plasma Phys. Control. Fusion 56 (10) (2014) 105004.

[22] J. Koenders, M. Wensing, T. Ravensbergen, O. Février, A. Perek, M. van Berkel, the TCV Team, the EUROfusion MST1 Team, Systematic extraction of a control-oriented model from perturbative experiments and SOLPS-ITER for emission front control in TCV, Nucl. Fusion 62 (6) (2022) 066025, http://dx.doi.org/10.1088/1741-4326/ac5b8c.

[23] M. Van Berkel, T. Kobayashi, H. Igami, G. Vandersteen, G. Hogeweij, K. Tanaka, N. Tamura, H. Zwart, S. Kubo, S. Ito, et al., New evidence and impact of electron transport non-linearities based on new perturbative inter-modulation analysis, Nucl. Fusion 57 (12) (2017) 126036.

[24] T. Ravensbergen, M. van Berkel, A. Perek, C. Galperti, B.P. Duval, O. Février, R.J. van Kampen, F. Felici, J.T. Lammers, C. Theiler, J. Schoukens, B. Linehan, M. Komm, S. Henderson, D. Brida, M.R. de Baar, Real-time feedback control of the impurity emission front in tokamak divertor plasmas, Nature Commun. 12 (1) (2021) 1–9, http://dx.doi.org/10.1038/s41467-021-21268-3.

[25] G. Witvoet, M. De Baar, E. Westerhof, M. Steinbuch, N. Doelman, Systematic design of a sawtooth period feedback controller using a Kadomtsev–Porcelli sawtooth model, Nucl. Fusion 51 (7) (2011) 073024.

[26] J. Koenders, A. Perek, B. Kool, O. Février, T. Ravensbergen, C. Galperti, B. Duval, C. Theiler, M. van Berkel, T. Team, et al., Model-based impurity emission front control using deuterium fueling and nitrogen seeding in TCV, Nucl. Fusion 63 (2) (2022) 026006.

[27] G.L. Derks, J.P.K.W. Frankemölle, J.T.W. Koenders, M. van Berkel, H. Reimerdes, M. Wensing, E. Westerhof, Benchmark of a self-consistent dynamic 1D divertor model DIV1D using the 2D SOLPS-ITER code, Plasma Phys. Control. Fusion 64 (12) (2022) 125013, http://dx.doi.org/10.1088/1361-6587/ac9dbd.

[28] S. Korving, G. Huijsmans, J.-S. Park, A. Loarte, J. Team, et al., Development of the neutral model in the nonlinear MHD code JOREK: Application to E× B drifts in ITER PFPO-1 plasmas, Phys. Plasmas 30 (4) (2023).

[29] T.C. Blanken, F. Felici, C.J. Rapson, M.R. de Baar, W.P. Heemels, Control-oriented modeling of the plasma particle density in tokamaks and application to real-time density profile reconstruction, Fusion Eng. Des. 126 (November 2017) (2018) 87–103, http://dx.doi.org/10.1016/j.fusengdes.2017.11.006.

[30] T.O. Bosman, O. Kudláček, E. Fable, M. van Berkel, F. Felici, A. Bock, T. Luda, M.R. de Baar, Kalman filter density reconstruction in ICRH discharges on ASDEX Upgrade, Fusion Eng. Des. 170 (April) (2021) http://dx.doi.org/10.1016/j.fusengdes.2021.112510.

[31] C.U. Schuster, E. Wolfrum, E. Fable, R. Fischer, M. Griener, B. Tal, C. Angioni, T. Eich, P. Manz, U. Stroth, et al., Edge transport and fuelling studies via gas puff modulation in ASDEX Upgrade L-mode plasmas, Nuclear Fusion 62 (6) (2022) 066035, http://dx.doi.org/10.1088/1741-4326/ac6072.